DIFFERENTIAL INTERFEROMETRIC SAR TECHNIQUES FOR GENERATION OF TERRAIN AND BUILDING DEFORMATION MAPS

Oscar Mora[1,2], Jordi J. Mallorquí [1], Riccardo Lanari [3]

[1] Universitat Politècnica de Catalunya (UPC)
Dept. Teoria del Senyal i Comunicacions (TSC)
Campus Nord UPC D3-211
Jordi Girona 1-3, 08034 Barcelona, Spain
E-mail: mallorqui@tsc.ucp.es

[2] Institut Cartogràfic de Catalunya (ICC)
Unitat de Teledetecció
Parc de Montjuïc
08038 Barcelona, Spain
E-mail: omora@icc.es

[3] Istituto per il Rilevamento Elettromagnetico dell'Ambiente (IREA)
Consiglio Nazionale delle Ricerche (CNR)
Via Diocleziano, 328 – 80124 Napoli, Italy
E-mail: lanari.r@irea.cnr.it

Keywords: SAR, radar, interferometry, subsidence, deformation

Abstract

In this paper, advanced techniques for the generation of terrain deformation maps using SAR (Synthetic Aperture Radar) data are presented. One of the algorithms estimates the linear and non-linear components of the displacement, the error of the Digital Elevation Model (DEM) used to cancel the topographic term from the interferograms, and the atmospheric artifacts. The input data is a set of spatial low resolution Differential Interferograms (multi-look data) and their associated coherence images. The algorithm has no theoretical restrictions with respect to the minimum number of required interferograms and their baseline dimensions. However, better results are obtained with large datasets of short baseline interferograms. The algorithm takes advantage of those pixels presenting a good coherence level in the whole set of interferograms, avoiding the rest affected by temporal decorrelation. Another algorithm has been developed to estimate the deformation respect to the ground of spatial high resolution structures, such as buildings. The main point is the calculation of the phase residue obtained by subtracting equivalent low and high resolution versions of Differential Interferograms. Using this information it is possible to obtain the deformation evolution of high coherent points, like buildings. These algorithms have been tested with ERS SAR data from an area of Spain and the city of Naples (Italy).

1. Introduction

When generating an interferogram by combining two SAR images, its phase increments can be expressed as:

$$\Delta\Psi_{int} = \Delta\Psi_{flat} + \Delta\Psi_{topo} + \Delta\Psi_{mov} + \Delta\Psi_{atmos} + \Delta\Psi_{noise} \quad (1)$$

where $\Delta\Psi_{flat}$ is the flat earth component related with range distance, $\Delta\Psi_{topo}$ is the topographic phase, $\Delta\Psi_{mov}$ is the component due to the displacement of the terrain in slant-range direction or Line of Sight (LOS) between both SAR acquisitions, $\Delta\Psi_{atmos}$ is the phase related with atmospheric artifacts, and $\Delta\Psi_{noise}$ comprises degradation factors such as spatial and temporal decorrelation.

The classical differential interferometric technique deals with the subtraction of the known components of equation (1) to obtain the phase related with terrain displacement. This can be achieved by generating the topographic phase using an external DEM and synthesizing the flat earth component with the orbital information. Nevertheless, these differential interferograms can be seriously affected by atmospheric artifacts, being impossible their study.

2. Linear and non-linear deformation of extended areas

The first part of the developed method assumes a linear deformation model of subsidence [1]. This means that we assume that the most important component of the movement during the observation time can be related with a constant velocity vector. Using a set of differential interferograms, the model can be fitted to the data taking advantage of the different time acquisition points. Nevertheless, before this processing, a selection of pixels based on their quality is necessary to reject points seriously affected by noise.

2.1 Pixel selection

The selection of quality pixels can be performed by making a temporal study of coherence images related with interferograms. This study can be carried out by calculating the mean coherence for each pixel taking into account the whole stack of interferograms:

$$\gamma_{\text{mean}} = \frac{1}{N} \cdot \sum_{i=0}^{N-1} \gamma_i \tag{2}$$

where N is the number of interferograms and γ_i is the coherence map for each interferogram. At this point, we have a temporal estimation of spatial coherence for each pixel within the image. A coherence threshold must be defined to select the high quality pixels and reject the low quality ones. By empirical analysis, we have found that a threshold of 0.25 is suitable for most of the applications.

2.2 Triangulation

The phase of individual pixels is not of practical utility due to the presence of different phase offsets among the differential interferograms, and it is not possible to link all this temporal information. These offsets could be calculated over high coherence stable areas not affected by subsidence and atmospheric artifacts, but in this case, additional input information will be required. This limitation can be overcome by relating two neighboring pixels, positioned at (x_m, y_m) and (x_n, y_n), by means of a Delaunay triangulation [2]. This triangulation consists on the non-overlapping triangles with vertices in the pixels and such that no pixels are enclosed by the circumscribing circles of any triangles. In this case, the differential phase increment between two neighboring pixels can be expressed as:

$$\begin{aligned} \Delta\Psi_{\text{dif}}(x_m, y_m, x_n, y_n, T_i) &= \frac{4\pi}{\lambda} \cdot T_i \cdot [v(x_m, y_m) - v(x_n, y_n)] + \\ &+ \frac{4\pi}{\lambda} \cdot \frac{B_n(T_i)}{r(T_i) \cdot \sin\alpha(T_i)} \cdot [\varepsilon(x_m, y_m) - \varepsilon(x_n, y_n)] + \\ &+ [\beta(x_m, y_m) - \beta(x_n, y_n)] + [\varphi(x_m, y_m) - \varphi(x_n, y_n)] + [n(x_m, y_m) - n(x_n, y_n)] \end{aligned} \tag{3}$$

where x and y are the pixel positions within the image, T_i is the time baseline of the *i-th* interferogram, λ is the wavelength, v is the constant velocity component of deformation (LOS), B_n the spatial baseline of the *i-th* interferogram, r the range distance, α the incidence angle, ε the topographic error of the DEM, β the non-linear component of the velocity, φ the atmospheric phase component, and n the decorrelation noise. Another advantage of relating neighboring pixels is that the atmospheric component is minimized for every relationship due to their spatial proximity. To reduce atmospheric artifacts, the distance between related pixels should not be larger than 1 Km, because this is approximately the correlation distance of atmosphere [1,3]. Obviously, the resulting values of velocity and topographic error will be expressed as increments between neighboring pixels.

2.3 Linear model adjustment

The expression of phase increment has a high number of unknowns, but basically we are interested in the determination of velocity and topographic error. A model based on these known variables can be constructed as follows:

$$\Delta\Psi_{\text{model}}(x_m, y_m, x_n, y_n, T_i) = \frac{4\pi}{\lambda} \cdot T_i \cdot [v_{\text{model}}(x_m, y_m) - v_{\text{model}}(x_n, y_n)] + \\ + \frac{4\pi}{\lambda} \cdot \frac{B_n(T_i)}{r(T_i) \cdot \sin\alpha(T_i)} \cdot [\varepsilon_{\text{model}}(x_m, y_m) - \varepsilon_{\text{model}}(x_n, y_n)] \quad (4)$$

A solution of velocity and topographic error increments can be obtained matching the data with the model. Taking into account that the atmospheric artifact component is very similar between neighboring pixels, its contribution will be negligible. The matching can be performed by a maximization process of the following *model fitting* function:

$$\Gamma(x_m, y_m, x_n, y_n) = \frac{1}{N} \cdot \left| \sum_{i=0}^{N} \exp[j \cdot (\Delta\Psi_{\text{dif}}(x_m, y_m, x_n, y_n, T_i) - \Delta\Psi_{\text{model}}(x_m, y_m, x_n, y_n, T_i))] \right| \quad (5)$$

where N is the number of interferograms. This function gets value one when the matching between the model and data is perfect and zero when decorrelation is total. Once this maximization process has been done for every relationship, the result is a set of velocity and topographic error increments for each pair of points.

2.4 Integration

Nevertheless, the velocity and topographic error increments are not the desired values, and an integration process is necessary to obtain the absolute values for each isolated pixel. This integration processing has been solved using a Region Growing (RG) based algorithm [4]. At this point we have a set of points spread over the area under study and connected by means of a Delaunay triangulation. We also have the differential values of velocity (Δv_{est}) and topographic error ($\Delta\varepsilon_{\text{est}}$) between connected pixels and a measurement of the quality of the model fitting function (Γ). Using all this information, integration of data can be performed weighting the quality of each differential value with its model fitting quality factor:

$$v_{\text{est}}(x, y) = \frac{1}{\sum_i \Gamma(x, y, x_i, y_i)} \cdot \sum_i [v_{\text{est}}(x_i, y_i) + \Delta v_{\text{est}}(x, y, x_i, y_i)] \cdot \Gamma(x, y, x_i, y_i) \\ \varepsilon_{\text{est}}(x, y) = \frac{1}{\sum_i \Gamma(x, y, x_i, y_i)} \cdot \sum_i [\varepsilon_{\text{est}}(x_i, y_i) + \Delta\varepsilon_{\text{est}}(x, y, x_i, y_i)] \cdot \Gamma(x, y, x_i, y_i) \quad (6)$$

where v_{est} and ε_{est} are the absolute values of velocity and topographic error respectively, Δv_{est} and $\Delta\varepsilon_{\text{est}}$ are the increment values between neighboring pixels, and Γ is the model fitting value.

2.5 Non-linear displacement and atmospheric artifacts estimation

We have previously seen the description of a method for obtaining the linear parameters (deformation velocity and topographic error) from a set of differential interferograms. Nevertheless, there is a component of the displacement that still remains unsolved. This component is the non-linear displacement, and must be added to the linear velocity to obtain the temporal evolution of deformation. The main problem we face when trying to estimate the non-linear component is the presence of atmospheric disturbances on the differential phase. For this reason, the estimation of the non-linear deformation is carried out in two steps; at Spatial Low Resolution (SLR) and Spatial High Resolution (SHR) in order to remove the atmospheric disturbances.

The first step of the algorithm is based on the calculation of the phase residues obtained by subtracting the linear deformation model to the original differential interferometric phases, as it is shown in the following equation:

$$\Delta\Psi_{\text{residue}}(x, y, T_i) = \Delta\Psi_{\text{dif}}(x, y, T_i) - \Delta\Psi_{\text{linear model}}(x, y, T_i) \quad (7)$$

where $\Delta\Psi_{\text{dif}}$ are the original differential phases and $\Delta\Psi_{\text{linear model}}$ are the phases generated with the linear deformation model previously obtained:

$$\Delta\Psi_{\text{linear model}}(x,y,T_i)=\frac{4\pi}{\lambda}\cdot T_i\cdot v(x,y)+\frac{4\pi}{\lambda}\cdot\frac{B_n(T_i)}{r(T_i)\cdot\sin\alpha(T_i)}\cdot\varepsilon(x,y) \tag{8}$$

After this procedure, the obtained residue can be expressed as:

$$\Delta\Psi_{\text{residue}}(x,y,T_i)=\Delta\Psi_{\text{non-linear}}(x,y,T_i)+\Delta\Psi_{\text{atmos}}(x,y,T_i)+\Delta\Psi_{\text{noise}}(x,y,T_i) \tag{9}$$

where we can see two important components; atmospheric artifacts ($\Delta\Psi_{\text{atmos}}$) and non-linear displacement ($\Delta\Psi_{\text{non-linear}}$). The third term ($\Delta\Psi_{\text{noise}}$) can be mainly associated to decorrelation and thermal noise. Our goal is to separate and obtain the components of atmosphere and non-linear displacement. Nevertheless, before estimating the non-linear deformation, we need to obtain the atmospheric phases of each differential interferogram.

Using the phase residue obtained in equation (9) we estimate the atmospheric artifacts taking advantage of their special frequency characteristics in space and time. Atmosphere can be considered as a low frequency signal in space; it has approximately 1 Km of correlation distance [1,3]. At the same time, it can be also considered as a high frequency signal in time, because for each acquisition date atmospheric conditions are a random variable (characteristics of troposphere are different from one day to another in a random way). On the other hand, the non-linear displacement can be assumed as a low frequency signal in time, if we consider that these variations are not totally random. Taking into account all this considerations, the estimation of the atmospheric artifacts can be performed by a filtering process in space and time.

The spatial filtering is carried out by applying a two-dimensional low pass filter with a correlation window of 1 Km x 1 Km (estimated correlation distance of atmosphere). After applying this filter, only two components remain:

$$\Delta\Psi_{\text{residue SLR}}(x,y,T_i)=\Delta\Psi_{\text{atmos}}(x,y,T_i)+\Delta\Psi_{\text{non-linear SLR}}(x,y,T_i) \tag{10}$$

where $\Delta\Psi_{\text{non-linear SLR}}$ is the non-linear component of the displacement at spatial low resolution (SLR) and it is assumed that atmosphere ($\Delta\Psi_{\text{atmos}}$) is not affected by the spatial filter. As atmospheric artifacts present a high frequency behavior in time, a temporal high pass filter can be applied to retrieve its contribution. The interferograms have been formed from the phases of two SAR images separated in time and, as noted before, none restriction has been applied on the pair selection. Consequently, the interferograms does not follow the temporal order required by the filter. The formation of the interferogram can be expressed in the following way:

$$\Delta\Psi_{\text{residue SLR}}(x,y,T_i)=\Delta\phi_{\text{residue SLR master}}(x,y,t_A)-\Delta\phi_{\text{residue SLR slave}}(x,y,t_B)\qquad\forall i=1,\ldots,N \tag{11}$$

where $\Delta\phi_{\text{residue SLR master}}$ and $\Delta\phi_{\text{residue SLR slave}}$ are the spatial low resolution residues of the master and slave SAR images at acquisition times t_A and t_B respectively, and $T_i=t_B-t_A$. Equation (11) if expressed as a system of equations can be solved to retrieve the phase contribution of each single image. In the most general case these SLR residual phases have to be unwrapped before solving the system. As these SLR residual phases present a low number of fringes (as it is composed by atmosphere, that is a signal with a low variation in space, and the spatial low resolution version of the non-linear displacement, that can be considered similar to atmosphere) the unwrapping process is extremely easy using classical methods. In this case, we have selected the LMS (Least Minimum Squares) method [5].

Once the SLR residues have been unwrapped we can solve the system of equations derived from (11). The matrix to invert is singular when disconnected subsets of interferograms, having no common SAR images, are present and the system will have an infinite number of solutions. To overcome this limitation we use the Singular Value Decomposition (SVD) that obtains the least square solution of minimum norm [6]. After this processing the residual phase belonging to each SAR image respect to the master is:

$$\Delta\phi_{\text{residue SLR}}(x,y,t_i)=\begin{cases}0 & i=0\\ \Delta\phi_{\text{atmos}}(x,y,t_i)+\Delta\phi_{\text{non-linear SLR}}(x,y,t_i) & 1\le i\le M-1\end{cases} \tag{12}$$

where M is the number of images. Finally, a temporal filtering is applied to isolate the atmospheric contribution and the non-linear deformation at low resolution.

Once we have calculated the linear and SLR non-linear deformation we can express the total displacement phase in the following way:

$$\phi_{\text{deformation}}(x,y,t_i) = \frac{4\pi}{\lambda}\cdot(t_i - t_0)\cdot v_{\text{est}}(x,y) + \phi_{\text{non-linear SLR}}(x,y,t_i) \tag{13}$$

But the real displacement has another additional term, the spatial high-resolution (SHR) non-linear deformation. This new component appears because we have omitted some information when filtering low-pass in space the original residues. The procedure to obtain the SHR component will be similar to the one used to estimate the atmospheric artifacts and the SLR displacement. The first step consists on the generation of a phase model with all the information available, in this case; linear deformation (v_{est}), SLR nonlinear displacement ($\phi_{\text{non-linear SLR}}$), DEM error (ε_{est}) and atmosphere (ϕ_{atmos}). A new residue can be obtained by subtracting this model to the original differential interferometric phases. The obtained residue will be basically composed by two terms: the SHR non-linear displacement and noise. The procedure to obtain the phase evolution of the SHR component will be similar to the one used to decompose the SLR residue using the SVD method.

Finally, the complete solution of deformation will be obtained adding all the components previously estimated. This information is expressed in radians (phase), and must be translated into distance (deformation) in the LOS:

$$\rho(x,y,t_i) = \frac{\lambda}{4\pi}\cdot\left[\frac{4\pi}{\lambda}\cdot(t_i - t_0)\cdot v_{\text{est}}(x,y) + \phi_{\text{non-linear SLR}}(x,y,t_i) + \phi_{\text{non-linear SHR}}(x,y,t_i)\right] \tag{14}$$

3. High-resolution structure deformation

The approach previously presented is designed to monitor deformations occurring at a relatively large spatial scale (pixel dimensions of the order of 100 m x 100 m). Nevertheless, it is not appropriate for analyzing local deformations that may affect, for example, small buildings suffering a structural stress. Accordingly, a new algorithm is proposed allowing to extend the monitoring capability of the SLR and SHR techniques to small scale deformations; in particular, the presented solution relies on small baseline interferograms and it is implemented by using two different sets of DIFSAR interferograms generated at low spatial resolution (multi-look data) and high resolution (single-look data), respectively. The former are used to identify, via the SLR and SHR approaches, possible atmospheric phase artifacts and the large scale deformation patterns, first; these signals are then subtracted modulo-2π from the high resolution data and, on the residual phase components, structures highly coherent in time (buildings, rocks, lava structures, etc.) are identified jointly to their local topography and the mean velocity of differential deformation. A final step, implemented again via the SVD technique, leads to the estimation of the temporal evolution of the local deformation affecting these high coherent structures.

The input data consists on a stack of single-look complex DIFSAR interferograms with short baselines. The first step of the algorithm implies the estimation and removal of the phase components related to the large spatial scale deformations and to possible topographic and atmospheric artifacts. The estimation of these phase components can be performed in two ways; using the results of deformation and atmosphere obtained with the SLR and SHR algorithms or performing a multi-look (spatial averaged) process of the one-look interferograms. Note that both methods must result in the same spatial low resolution phases composed by deformation, topographic error and atmosphere. Following this estimation operation, the obtained signals are subtracted modulo-2π from the high resolution data; thus, the residual phase component will only account for differential deformation phenomena with respect to the previously estimated (if present) large scale displacement. In particular, the residual phase of each pixel within the *i-th* single-look interferogram can be expressed as follows:

$$\Delta\Psi_{\text{residue}}(x,y,T_i) = \Delta\Psi_{\text{def small scale}}(x,y,T_i) + \Delta\Psi_{\text{topo small scale}}(x,y,T_i) + \Delta\Psi_{\text{noise}}(x,y,T_i) \tag{15}$$

where $\Delta\Psi_{\text{def small scale}}$ is the interferometric phase related with the deformation at small scale, such as the displacement of a building, and $\Delta\Psi_{\text{topo small scale}}$ is the residue obtained by subtracting the large and small scale versions of the topographic error. We explicitly note that the deformation signal decoupling into a linear and a non-linear component is related to the implementation of the residual phase unwrapping operation, which is needed because only the wrapped component of the signal can be directly computed from the SLC data. Accordingly, the following phase unwrapping strategy is considered; we estimate first the terms $v_{\text{small scale}}$ and $\varepsilon_{\text{small scale}}$ via the maximization of the following model fitting function:

$$\Gamma(x,y)=\frac{1}{N}\cdot\left|\sum_{i=0}^{N}\exp\left[j\cdot\left(\Delta\Psi_{\text{residue}}(x,y,T_i)-\Delta\Psi_{\text{model}}(x,y,T_i)\right)\right]\right| \tag{16}$$

where N is the number of differential interferograms and $\Delta\Psi_{\text{model}}$ is the phase linear model equivalent to equation (8). Following the estimation of the factors velocity and topographic error via the maximization of (16), the final step of the procedure consists on the full determination of the time evolution of the deformations affecting those pixel exhibiting a value of the factor greater than a fixed threshold. This result can be achieved by subtracting the model from the original differential interferometric phase, thus obtaining a new residual phase signal related to the non-linear component of the differential deformation velocity. Applying again the SVD method, the non-linear term of the displacement is obtained, and the deformation evolution of high resolution structures can be expressed as:

$$\rho_{\text{small scale}}(x,y,t_i)=\frac{\lambda}{4\pi}\cdot\left[\frac{4\pi}{\lambda}\cdot(t_i-t_0)\cdot v_{\text{small scale}}(x,y)+\phi_{\text{non-linear}}(x,y,t_i)\right] \tag{17}$$

4. Experimental results

Two areas have been selected to test the methods previously presented with ERS data: the first one corresponds to an area of Spain affected by localized problems of subsidence, while the second one belongs to the city of Naples and its surroundings (Italy).

The linear and non-linear deformation for extended areas algorithm has been applied to a set of images from the area of Spain. Figure 1 shows the linear deformation and topographic error maps obtained over the area under study (10 Km x 16 Km) using a stack of 28 short baseline interferograms. Results show that nearly all the selected pixels present no deformation. Nevertheless, the algorithm has detected a small area in the upper part of the image with significant subsidence (up to 1.8 centimeters per year in the LOS). Due to the usage of short baselines the estimation of DEM errors is not very precise. Figure 2 shows details of two main zones; the one affected by subsidence problems and an stable area.

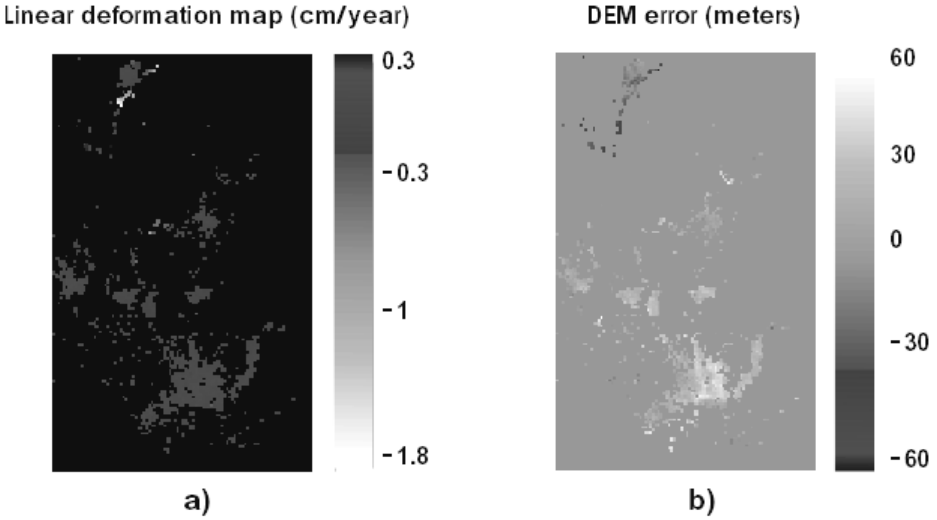

Figure 1: Velocity (centimeters per year) (a) and topographic error (meters) (b) maps over selected coherent points. Most of the points have approximately zero velocity of deformation, as it was expected. Only two small parts on the north present deformations up to 1.8 centimeters per year.

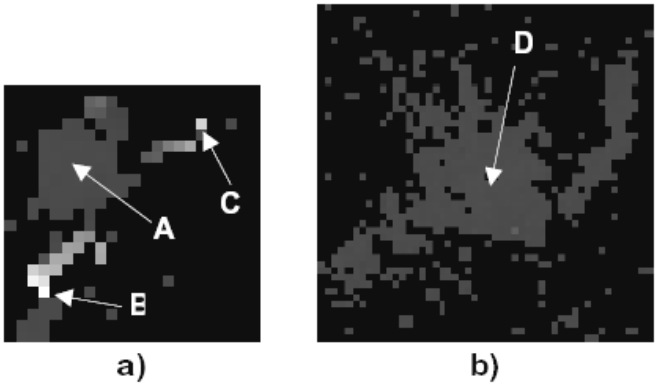

Figure 2: Zooms of interesting areas. Points with no deformation (A and D) and points affected by subsidence (B and C).

Applying the techniques for the detection of the non-linear deformation component, the complete deformation plot is obtained for each pixel. Figure 3 shows the displacement evolution for the points depicted in Figure 2. The *Institut Cartogràfic de Catalunya* (ICC) has provided information to confirm these deformation rates in the area under study.

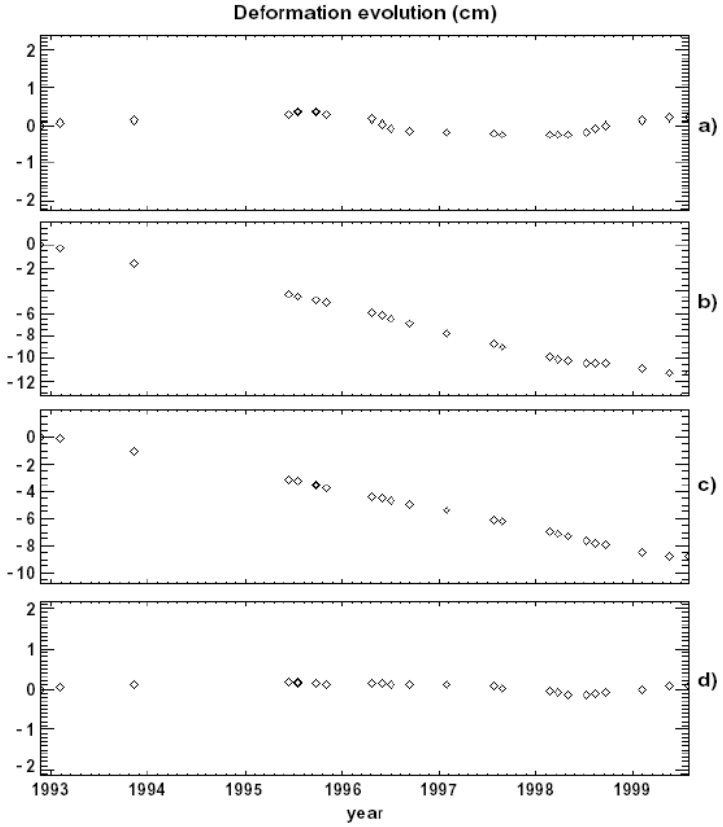

Figure 3: Deformation evolution plots of the studied points. The stable points, (a) and (d), only present a small deviation of a few millimeters from the zero deformation line. The result is similar for points (b) and (c), with a perfect linear trend. Only point (b) has a slight non-linear deformation pattern at the beginning of 1998, where the displacement seems to reduce its velocity.

A stack of 70 short baseline differential interferograms has been selected for the study of structure stability in the city of Naples (Italy). Figure 4 depicts details of a very small zone of the city containing a metallic building. Several points have been detected over the same structure. This building has been selected due to the difficulty to find leveling measurements of buildings deforming. The reason of this selection is that these metallic structures are affected by important thermal deformations that can be detected using the presented method. Figure 6 shows the deformation evolution in time for three points of this building. All of them present a high correlation with temperature measurements, higher than 0.8. Another example is shown in Figure 7, where displacement evolution of two points of another building of the city is presented. In this case no measurements are available for validation. Nevertheless, results obtained from thermal deformation encourage us for the validity of the algorithm.

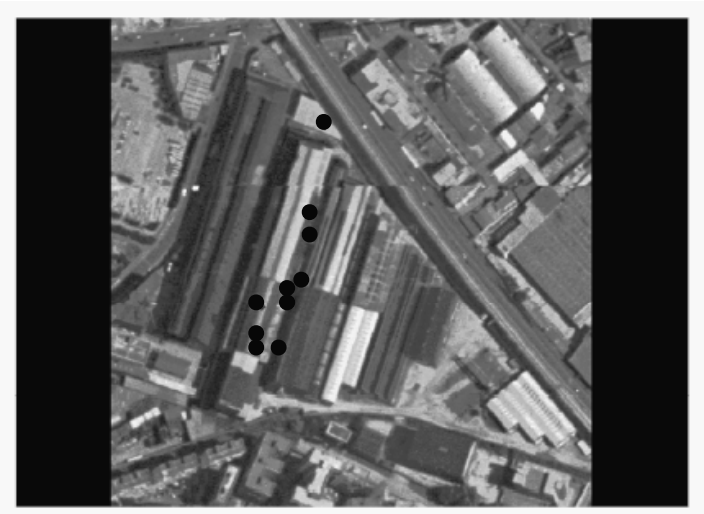

Figure 4: Points selected over a metallic building. Metallic structures can be affected by deformation proportional to thermal changes.

Figure 5: Photographs of the building affected by thermal deformation. Note the metallic structure of the building.

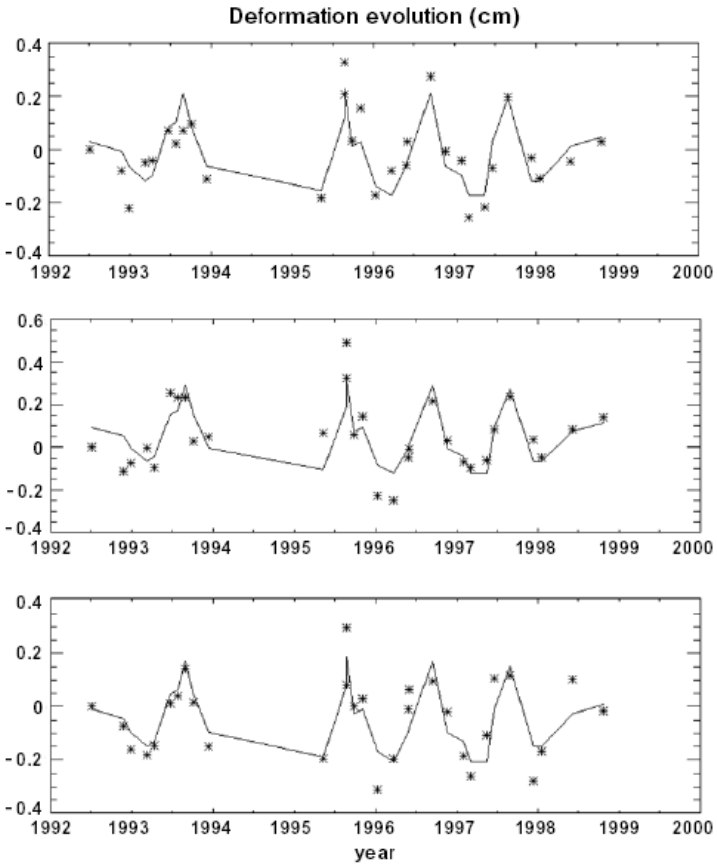

Figure 6: Deformation evolution plots of three points of the studied building compared with a scaled version of temperature changes. In all the cases the correlation between deformation and temperature is greater than 0.8.

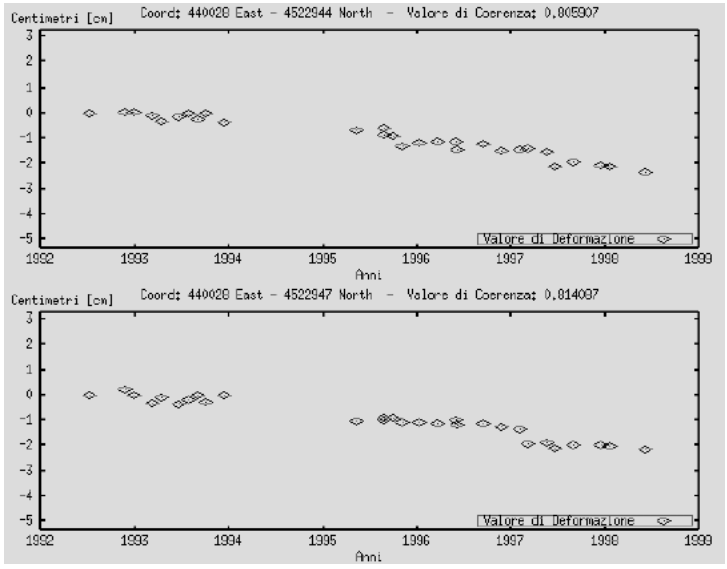

Figure 7: Deformation plots of two points that belong to the same building.

9. Acknowledgment

The authors would like to thank the European Space Agency (ESA) for providing the ERS images used in this work under the EO Projects of category 1 (A03.421) and the CICYT TIC 1999-1050-C03-01 for the economical support to the project. Fundación Repsol for providing the first two years of pre-doctoral fellowship. The CIRIT (Catalan Commission for Research) for providing the last two years of pre-doctoral fellowship needed for the fulfillment of the Thesis. This work has been also partially sponsored by the Italian Space Agency and the National Group of Volcanology (GNV). The precise ERS-1/ERS-2 satellite orbit state vectors for the study of the city of Naples have been provided by the University of Delft, The Netherlands.

References

[1]. A. Ferretti, C. Prati and F. Rocca. Nonlinear subsidence rate estimation using Permanent Scatterers in Differential SAR Interferometry. IEEE Transactions on Geoscience and Remote Sensing, Vol. 38, No. 5, September 2000.
[2]. B. Delaunay. Sur la sphere vide. Bulletin of Academy of Sciences of the USSR, pp. 793-800, 1934.
[3]. R. Hanssen. Atmospheric heterogeneities in ERS Tandem SAR Interferometry. Delft, The Netherlands: Delft Univ. Press, 1998.
[4]. W. Xu, W. and I. Cumming. Region Growing Algorithm for InSAR Phase Unwrapping. Proceedings of IGARSS'96, Lincoln, Nebraska, pp. 2044-2046.
[5]. D.C. Ghiglia, L.A. Romero. Robust two-dimensional weighted and unweighted phase unwrapping that uses fast transforms and iterative methods. J. Opt. Soc. Am. Vol.11, No.1, pp. 107-117, January 1994.
[6]. P. Berardino et al. A new approach for analyzing the temporal evolution of Earth surface deformations based on the combination of DIFSAR interferograms. Proceedings of International Geoscience and Remote Sensing Symposium (IGARSS 2001), Sydney, Australia, July 9-13, 2001.
[7]. O. Mora, J. J. Mallorquí, J. Duro. Generation of deformation maps at low resolution using differential interferometric SAR data. Proceedings of International Geoscience and Remote Sensing Symposium (IGARSS 2002), Toronto, Canada, June 24-28, 2002.
[8]. O. Mora, R. Lanari, J. J. Mallorquí, P. Berardino, E. Sansosti. A new algorithm for monitoring localized deformation phenomena based on small baseline differential SAR interferograms. Proceedings of International Geoscience and Remote Sensing Symposium (IGARSS 2002), Toronto, Canada, June 24-28, 2002.